
The Influence of Tracer Localization on the Electron Dose Rate Delivered to the Cell Nucleus

Marc Faraggi, Isabelle Gardin, Claire de Labriolle-Vaylet, Jean-Luc Moretti and Bernard D. Bok

Nuclear Medicine Department, Bichat Hospital, Paris; Nuclear Medicine Department, Beaujon Hospital, Clichy; Nuclear Medicine Department, Saint Antoine Hospital, Paris; and Nuclear Medicine Department, Avicenne Hospital, Bobigny, France

The radiation dose rate delivered by electron emissions of ^{99m}Tc , ^{123}I , ^{111}In , ^{67}Ga and ^{201}Tl was evaluated at the subcellular level. **Methods:** Spherical models of sources were used to simulate various cellular localizations of radionuclides. These models were applied to large lymphocytes, assuming uniform distributions of radioactivity throughout the nucleus, the cytoplasm or the cell membrane surface. **Results:** The graphs of the absorbed dose rate plotted according to the distance from the center of the cell show that the dose rate strongly depends on the subcellular distribution of the radioisotope. The absorbed dose rate $\dot{D}(0)$ at the center of the cell delivered by a constant cellular radioactivity of ^{99m}Tc , ^{123}I , ^{111}In , ^{67}Ga and ^{201}Tl is respectively 94, 21, 18, 74 and 76 times higher if the radioactivity is localized within the cell nucleus than if it is situated only on the cell membrane. $\dot{D}(0)$ for subcellular localizations was compared to $\dot{D}(0)$ obtained by assuming uniform distribution of radioactivity throughout the cell. This latter assumption may underestimate the dose rate from 2.8- to 3.2-fold if the tracer is exclusively localized within the nucleus or overestimate from 4.3- to 30-fold if the tracer is localized within the cytoplasm or on the cell membrane, depending on the radionuclide. **Conclusion:** Such findings show that the localization of radiopharmaceuticals at the subcellular level plays a crucial role in determining the actual dose delivered to the cell nucleus in diagnostic nuclear medicine procedures.

Key Words: dose rate; electron; microdosimetry; diagnostic; intracellular distribution; radiopharmaceuticals

J Nucl Med 1994; 35:113-119

Most photon emitters used in diagnostic nuclear medicine procedures also emit electrons (internal conversion, Auger, Coster-Kronig). The absorbed dose at the cellular

level may be substantial if cellular uptake of such radionuclides remains stable in the course of time (1). Actually, low-energy electrons with cellular or subcellular ranges generate dose heterogeneity (2,3). Thus, dose calculation at the cellular level is more accurate than conventional dosimetry, as pointed out by Makrigiorgos et al. (4). These authors have shown that the radiation dose evaluated by conventional dosimetry may underestimate the dose actually delivered at the cellular level from a range of twofold up to more than 25-fold if the energy of the emitted electrons is less than 10 keV. For instance, the dose delivered to labeled Kupffer cells after ^{99m}Tc -sulphur colloid hepatic scintigraphy may reach 0.5 to 0.9 Gy/MBq (5). This represents about 15,000 times the electron dose estimated by conventional dosimetry. The dose to lymphocytes after leukocyte labeling has been evaluated up to 7 Gy when incubating 10^8 cells with 37 MBq ^{99m}Tc -pyrophosphate (6). Radiobiological implications are not negligible and evidence of chromosomal aberrations have been described when labeling lymphocytes not only with ^{111}In -oxinate (7) but also with ^{99m}Tc -pyrophosphate (8).

Dosimetric evaluations at the cellular level generally assume a uniform distribution of the radionuclide over the whole cell (1,4,5). Such an assumption is not always verified and radionuclides may get incorporated into the genetic material of the cell (9). Rao et al. (10) have demonstrated that spermhead survival and abnormalities depend on subcellular distribution of incorporated radionuclides. Furthermore, Hofer (11) has shown that the dose delivered to the cell nucleus is strongly dependent on intracellular radiotracer localization, which indicates the importance of such biological parameters.

The aim of this study was to evaluate the influence of the subcellular localization of ^{99m}Tc , ^{123}I , ^{111}In , ^{67}Ga and ^{201}Tl on the dose rate delivered to the cell and in particular to the nucleus. The dosimetric model has been designed for uniform distributions of radioactivity throughout the nucleus, cytoplasm or the cell membrane surface.

Received Apr. 9, 1993; revision accepted Sept. 28, 1993.
For correspondence and reprints contact: M. Faraggi, MD, PhD, Nuclear Medicine Department, Hôpital Bichat, 46, rue Henri Huchard, F 75018 Paris, France.

TABLE 1
Average Electron Energies E_i in keV and Yields n_i per Decay*

^{90m}Tc		^{123}I		^{111}In		^{67}Ga		^{201}Tl	
E_i	n_i	E_i	n_i	E_i	n_i	E_i	n_i	E_i	n_i
0.0334	1.98	0.006	2.18	0.00847	7.82	0.0624	2.07	0.0161	17.6
0.0429	0.0193	0.0298	2.10	0.0388	2.54	0.0729	0.346	0.0453	2.84
0.116	0.747	0.0325	6.54	0.125	0.915	0.921	1.68	0.0644	7.93
0.226	1.10	0.127	0.869	0.183	0.151	0.953	0.0116	0.172	4.41
1.82	0.991	0.213	0.156	0.350	2.09	7.43	0.470	0.406	0.923
2.05	0.0868	0.461	1.97	2.59	0.835	8.44	0.116	0.773	0.322
2.32	0.0137	3.04	0.751	3.06	0.190	9.46	0.0082	0.895	0.608
2.66	0.0012	3.66	0.202	3.53	0.0109	81.6	0.0027	1.83	2.03
15.3	0.0126	4.28	0.013	19.1	0.103	83.7	0.270	7.58	0.541
17.8	0.0047	22.4	0.0838	22.3	0.0394	92.2	0.0376	9.85	0.235
119	0.0843	26.3	0.0384	25.5	0.0036	93.2	0.0066	12.0	0.0191
122	0.0059	30.2	0.0035	145	0.0824	175	0.0034	12.2	0.0022
137	0.0136	127	0.130	167	0.01	291	0.001	15.9	0.0861
140	0.0062	154	0.0179	171	0.0014			17.4	0.0724
		158	0.0053	219	0.0521			27.7	0.0236
				241	0.0091			29.4	0.0237
				245	0.0019			52.2	0.0797
								55.0	0.0268
								66.3	0.0153
								77.5	0.0015
								82.8	0.0025
								84.3	0.159
								121	0.0152
								133	0.0027
								153	0.0269
								165	0.0094

*From Howell (17).

METHODS

Spherical models were used to estimate cellular distribution of the radiation dose rate delivered by electron emissions. Three source distributions were chosen to simulate various subcellular localizations of radionuclides:

1. The full sphere for radioactivity distributed throughout the entire cell or within the nucleus.
2. A void central sphere surrounded by a spherical ring simulating cytoplasmic distribution.
3. The sphere surface for localization on the cell membrane.

This model was applied to simulated large lymphocytes, with a nuclear radius q_n of 4 μm and a cell radius q_c of 6 μm (12).

The averaged dose rate was evaluated in two steps at each point of the cell on a IBM-compatible computer. First, the dose rate, \dot{D} , was calculated with the hypothesis of an isotropic point source. Second, extensive sources simulating subcellular localizations were considered. In each case, the study was performed assuming uniform distribution of radioactivity, isotropic emission of the electrons and a mean density, ρ , over the entire cell of 1 $\text{g} \cdot \text{cm}^{-3}$.

In the case of an isotropic point source and a spectrum of m monoenergetic electron emissions, \dot{D} (cGy/s) at a distance r (cm) of the point source may be expressed as (13):

$$\dot{D}(r) = Ak \sum_{i=1}^m n_i E_i \Phi_i(r, E_i),$$

where Φ_i is the i th specific absorbed fraction (g^{-1}); A is the source activity (Bq); E_i is the energy of the i th emission (MeV); n_i is the number of emitted electrons by disintegration; and $k = 1.6 \cdot 10^{-8} \text{g} \cdot \text{cGy} \cdot \text{MeV}^{-1}$.

To estimate Φ_i , we used the analytical functions published by Prestwich and Kwok (14,15) to compute the scaled electron dose point kernels tabulated by Berger (16). Details of these calculations are given in the Appendix. The radiation spectra for electron emissions (Table 1) were taken from Howell (17).

In order to calculate the absorbed dose rate for extensive sources, the dose rate evaluated with the assumption of the isotropic point source was integrated over the entire radioactive distribution (see Appendix). For the spherical source, an analytical method based on the geometric reduction factor proposed by Berger (13) was used. For the hollow sphere (i.e., the cytoplasm), the calculation was simply performed by subtracting the contribution of a sphere of radius q_n from the contribution of a sphere of radius q_c . For distribution on the cell membrane, the dose rate was directly integrated over the spherical surface, as published by Langmuir (18).

RESULTS

For cell size $q_n = 4 \mu\text{m}$ and $q_c = 6 \mu\text{m}$, the absorbed dose rate \dot{D} at any point of the cell is plotted according to the distance to the center of the nucleus. Figures 1 and 2 refer to uniform distribution of the five radionuclides respectively throughout the nucleus and cytoplasm for a

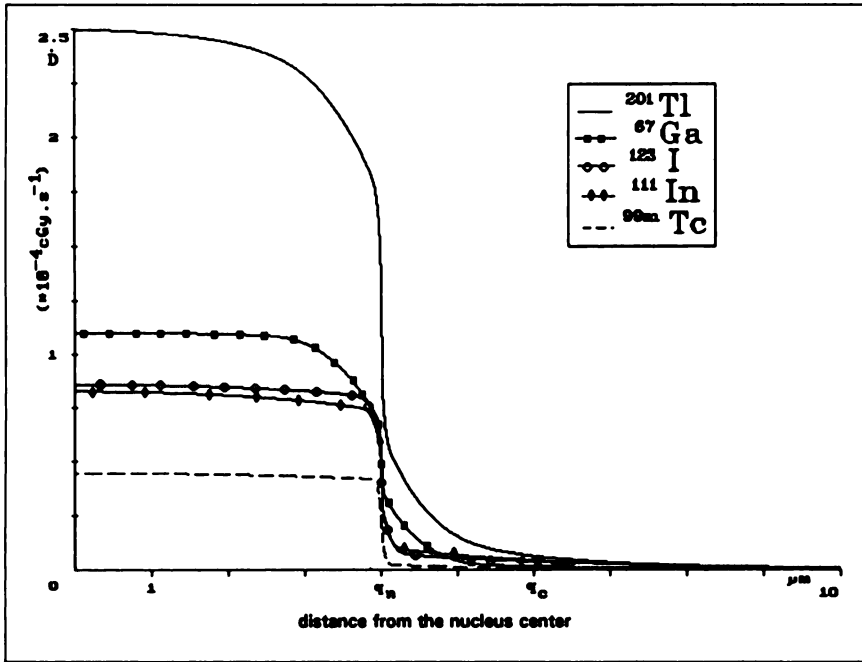


FIGURE 1. Dose rate \dot{D} versus the distance from the nuclear center of a large lymphocyte for uniform distribution of $1 \text{ MBq} \cdot \text{cm}^{-3}$ throughout the cell nucleus of $^{99\text{m}}\text{Tc}$, ^{123}I , ^{111}In , ^{67}Ga or ^{201}Tl .

volume activity of $1 \text{ MBq} \cdot \text{cm}^{-3}$. The curves in Figure 3 are drawn for $1 \text{ MBq} \cdot \text{cm}^{-2}$ of $^{99\text{m}}\text{Tc}$ and ^{201}Tl uniformly distributed on the cell membrane surface. Only two of the five radionuclides are plotted, but the shape of the curves is identical for all of them, showing a narrow peak centered on the cell membrane. Data in Tables 2 and 3 represent the dose rates found with the three source distributions at the center of the nucleus $\dot{D}(0)$ and at the cell membrane $\dot{D}(q_c)$.

The influence of localization in comparison with uniform distribution throughout the cell is shown in Table 4. Listed

in this table are the ratios between the dose rate to the nucleus center $\dot{D}(0)$ computed for the three tracer localizations (nucleus, cytoplasm and cell membrane) to the dose rate $\dot{D}(0)$ calculated for a distribution throughout the cell. The total amount of radioactivity is assumed to be the same in each case.

If total cellular radioactivity in a large lymphocyte remains constant, the absorbed dose rate $\dot{D}(0)$ at the center of the cell delivered by $^{99\text{m}}\text{Tc}$, ^{123}I , ^{111}In , ^{67}Ga and ^{201}Tl is respectively 94, 21, 18, 74 and 76 times higher for nucleus distribution than for cell membrane distribution.

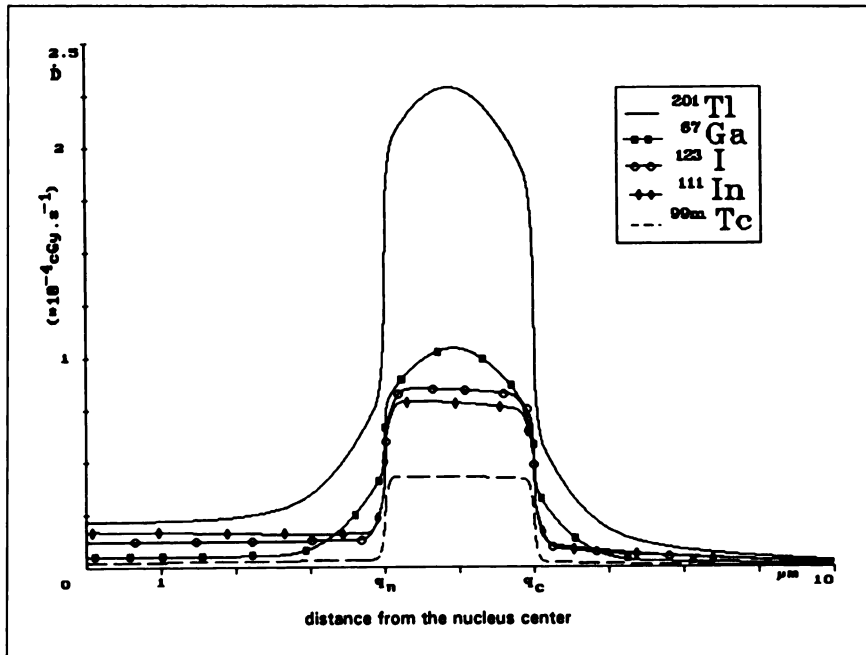


FIGURE 2. Dose rate \dot{D} versus the distance from the nuclear center of a large lymphocyte for uniform distribution of $1 \text{ MBq} \cdot \text{cm}^{-3}$ throughout the cell cytoplasm of $^{99\text{m}}\text{Tc}$, ^{123}I , ^{111}In , ^{67}Ga or ^{201}Tl .

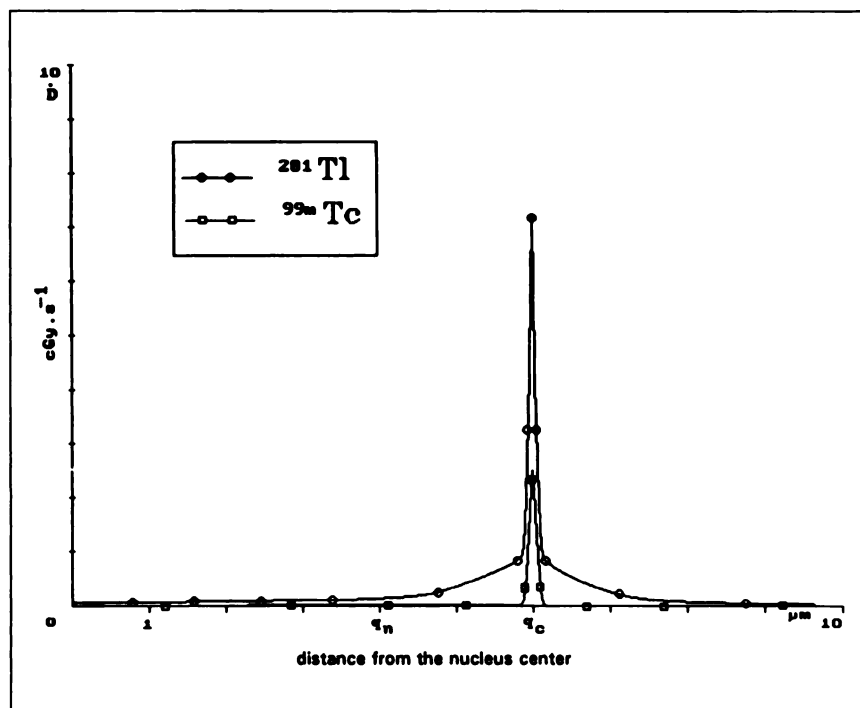


FIGURE 3. Dose rate \dot{D} versus the distance from the nuclear center of a large lymphocyte for uniform distribution of $1 \text{ MBq} \cdot \text{cm}^{-2}$ on the cell membrane of $^{99\text{m}}\text{Tc}$ or ^{201}Tl .

DISCUSSION

Spherical geometry is an oversimplified model of the cell and cell nucleus shapes, which may be very irregular. However, an excellent fit was obtained with the lymphocytes, which were chosen as an example. This model may also be conveniently used on a PC.

In this study, we considered electron emissions only. The absorbed fraction of photon emissions to the labeled cells is very small, and the photonic contribution to the total absorbed dose may be neglected. For example, absorbed dose calculations (19) indicate that photons deposit less than 1% of the total lymphocyte dose during leukocytes labeling with $^{99\text{m}}\text{Tc}$ -HMPAO.

To calculate electron range and the energy delivered along their path, analytical functions proposed by Prestwich and Kwok (14) were used to fit the data published by Berger in 1973 (16). This model was previously validated for the electron emissions of the five radionu-

clides studied (20). A revision of Berger's values was recently proposed by Simpkin et al. (21). Differences between these two data sets are small when energy-loss straggling is negligible (21). Thus, the analytical method is in good agreement with these two reports.

Howell has evaluated at $1.60 \times 10^8 \text{ Gy/Bq} \cdot \text{h}$ the dose per unit cumulated activity to 20-nm diameter spheres containing uniformly distributed ^{125}I (17). We obtained $1.52 \times 10^8 \text{ Gy/Bq} \cdot \text{h}$ with the same spectrum. These values are in good agreement. The small difference (5%) may be attributed to the analytical methods used to compute the specific absorbed fraction. Howell et al. (22) calculated Φ from Cole's energy loss expression (23).

For the radionuclides studied, different spectra have been proposed in the literature (24,25,17). The absence of low-energy Auger electrons in spectra (24,25) results in significant differences in doses calculated at the subcellular level when the target studied is smaller than $1 \mu\text{m}$, as pointed out by Howell (17).

TABLE 2
Dose rate to the Center of a Large Lymphocyte for Uniform Distribution of $1 \text{ MBq} \cdot \text{cm}^{-3}$ Throughout the Nucleus or the Cell Cytoplasm and $1 \text{ MBq} \cdot \text{cm}^{-2}$ on the Cell Membrane

Tracer location	$^{99\text{m}}\text{Tc}$	^{123}I	^{111}In	^{67}Ga	^{201}Tl
Nucleus ($10^{-5} \text{ cGy} \cdot \text{s}^{-1}$)	4.5	8.6	8.3	11.0	25.4
Cytoplasm ($10^{-5} \text{ cGy} \cdot \text{s}^{-1}$)	0.2	1.2	1.7	0.5	2.2
Membrane ($10^{-2} \text{ cGy} \cdot \text{s}^{-1}$)	0.8	6.9	7.9	2.5	5.7

TABLE 3
Dose Rate $\dot{D}(q_c)$ to the Cell Membrane of a Large Lymphocyte for Uniform Distribution of $1 \text{ MBq} \cdot \text{cm}^{-3}$ Throughout the Nucleus or the Cell Cytoplasm and $1 \text{ MBq} \cdot \text{cm}^{-2}$ on the Cell Membrane

Tracer location	$^{99\text{m}}\text{Tc}$	^{123}I	^{111}In	^{67}Ga	^{201}Tl
Nucleus ($10^{-5} \text{ cGy} \cdot \text{s}^{-1}$)	0.08	0.39	0.44	0.16	0.64
Cytoplasm ($10^{-5} \text{ cGy} \cdot \text{s}^{-1}$)	2.53	5.58	5.09	5.47	13.8
Membrane ($\text{cGy} \cdot \text{s}^{-1}$)	2.49	2.06	2.32	3.85	7.19

TABLE 4

Ratio Between the Dose Rate $\dot{D}(0)$ to the Nucleus Center for Nucleus, Cytoplasm and Cell Membrane Localizations Versus Homogeneous Distribution over the Entire Cell

	^{201}Tl	^{111}In	^{123}I	^{67}Ga	$^{99\text{m}}\text{Tc}$
$\frac{\dot{D}(0)_{\text{nucleus}}}{\dot{D}(0)_{\text{cell}}}$	3.2	3.0	2.8	3.2	3.1
$\frac{\dot{D}(0)_{\text{cytopla.}}}{\dot{D}(0)_{\text{cell}}}$	0.068	0.17	0.23	0.056	0.10
$\frac{\dot{D}(0)_{\text{memb.}}}{\dot{D}(0)_{\text{cell}}}$	0.034	0.14	0.16	0.043	0.041

Total activity is the same for all the localizations.

One advantage of this method is that the calculation of monoenergetic dose point kernels and dose rate at any point may be easily performed on a PC. Only dose rates at the center of the sphere and on its surface are shown in Tables 2 and 3 for clarity. It may be noticed on the curves (Figs. 1-3) that there are no large variations in dose rates throughout the entire nucleus with all radionuclides, except at the external border.

The cell sizes in Figures 1 through 3 were chosen to be $q_c = 6 \mu\text{m}$ and $q_n = 4 \mu\text{m}$ to simulate large lymphocytes. These values are reasonable and were chosen just to illustrate the graphs. It could be noticed that the shapes of the curves would remain quite unchanged for other values of q_c and q_n . For a nuclear distribution of the tracer (Fig. 1), the dose rate \dot{D} , almost constant along the major central part of the nucleus, drops strongly at the edge of the nucleus and nearly vanishes in the cell cytoplasm. The plateau corresponding to the nucleus area may be explained by low-energy electrons that deposit their energy locally. The dose delivered to the cytoplasm is exclusively due to electrons of an energy higher than 10 keV. The reverse pattern is observed for exclusive cytoplasmic distribution of radionuclides (Fig. 2), where the dose delivered to the nucleus comes from electrons of energy higher than 10 keV. These results are in agreement with the dose rate profiles found by Rao et al. for ^{125}I distributed uniformly in the cell nucleus or in the cytoplasm (26).

When the tracer is localized on the cell membrane (Fig. 3), the shape of the curves is a narrow peak centered on the membrane, then \dot{D} drops down on both sides of this interface. There is clearly an overdose to the cell membrane as compared to the other cellular components. However, the dose rate $\dot{D}(0)$ at the center of the nucleus is not negligible.

In the particular example of $q_c = 6 \mu\text{m}$ and $q_n = 4 \mu\text{m}$ (i.e., a large lymphocyte), the values of $\dot{D}(0)$ are reported in Table 2. Table 2 shows that $\dot{D}(0)$ is maximum for ^{201}Tl , followed by ^{67}Ga , ^{123}I , ^{111}In and $^{99\text{m}}\text{Tc}$ for a localization into the cell nucleus. For cytoplasm and cell membrane localizations, the order is ^{201}Tl , ^{111}In , ^{123}I , ^{67}Ga and $^{99\text{m}}\text{Tc}$.

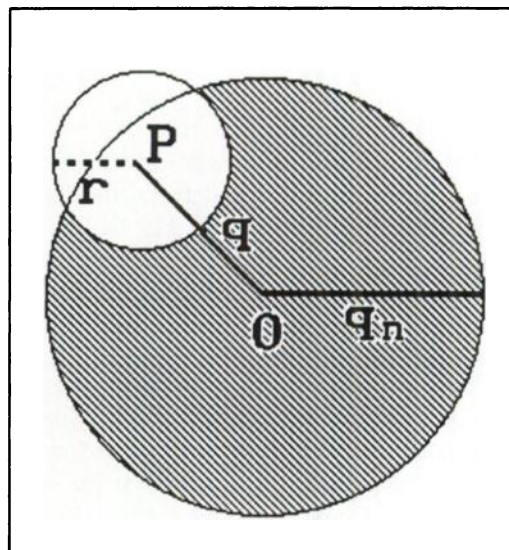


FIGURE 4. Geometry used for calculation of the reduction factor $\Omega(q, r, q_n)$. The sphere (center O, radius q_n) represents a cell nucleus containing a spherical homogeneous distribution of radioactivity. The observation point P is located at a distance q from O. The variable r represents the distance traveled by radiation emanating from the spherical shell of radius r to the center P.

Hofer et al. (11) have shown that the dose delivered to the cell nucleus depends on intracellular radiotracer localization. In particular, the nucleus seems to be a highly radiosensitive target in the cell. Assuming the same amount of radioactivity is delivered to a large lymphocyte, it is interesting to compare the $\dot{D}(0)$ obtained at the center of the nucleus for several distributions. If the uptake occurs within the nucleus only, then $\dot{D}(0)$ is underestimated by a factor of 2.8 to 3.2, depending on the radionuclide (Table 4) as compared to $\dot{D}(0)$ resulting from uniform distribution. This may be partially related to the differences of radioactive concentrations since the ratio between the volumes of the nucleus and the entire cell is 3.4. In contrast, if the tracer is localized throughout the cytoplasm or on the cell membrane, $\dot{D}(0)$ is overestimated from 4.3-fold (^{111}In localized throughout the cytoplasm) to 29.6-fold ($^{99\text{m}}\text{Tc}$ localized on the cell membrane), while the ratio between cell and cytoplasm volume is 1.42. This ratio may be favorable for radiopharmaceuticals that do not cross over the membrane of the nucleus.

Radiobiological results have shown the influence of tracer localization on cell survival (11). In particular, Narra and Rao (27,10) have demonstrated that spermhead survival and abnormalities in mouse testes induced by incorporated Auger emitters (^{123}I , ^{125}I and ^{111}In) depend on subcellular localization of the radionuclide. In contrast, subcellular distribution of beta emitters, such as ^{131}I , plays no role in determining their lethality (27). Rao et al. (26) have pointed out that dosimetric computations alone are unable to predict radiobiological consequences of ^{125}I incorporated into spermatogonial cells. Nevertheless, knowledge of the dose actually delivered at the subcellular

level is prerequisite to a better understanding of any dose effect relationship.

CONCLUSION

Several recent studies have shown that the tissue-averaged dose may considerably underestimate the dose received by certain cell components. For the five radionuclides studied, intracellular localization of tracer must be considered to calculate the average dose actually delivered to the nucleus of a cell population. Neglecting subcellular localization of a radiopharmaceutical may lead to underestimating or overestimating the dose rate and thus the dose to the nucleus. Even if dosimetry alone is not sufficient for predicting radiobiological effects, it may be of great importance to reach accurate dose estimates at the subcellular level to study cell survival of Auger emitters as a function of the absorbed dose.

APPENDIX

Dose rate was calculated with the assumption of the isotropic point source by first computing the specific absorbed fraction $\Phi(r, E)$ for each monoenergetic electron emission. To estimate $\Phi(r, E)$, analytical functions published by Prestwich and Kwok (14, 15) were used to compute the scaled electron dose point kernels $F(x)$ tabulated by Berger (16). x is a dimensionless quantity representing the ratio of the distance r to the electron range. The relationship between F and Φ for an electron of energy E is given by:

$$F(x, E) \cdot dx = 4\pi\rho r^2\Phi(r, E) \cdot dr.$$

For a spectrum of m monoenergetic electrons, the different components of the emitted radiations were taken into account to compute $\sum_{i=1}^m n_i E_i \Phi_i(r)$ and thus $\dot{D}(r)$.

For extensive sources, the dose rate $\dot{D}(r)$ evaluated with the assumption of the isotropic point source was integrated over the entire radioactive distribution to obtain the dose rate $\dot{D}(q)$ at a distance q from the center of the cell. For spherical distributions, $\dot{D}(q)$ may be expressed as:

$$\dot{D}(q) = 4\pi \frac{dA}{dV} k \sum_{i=1}^m n_i E_i \int_0^\infty \Phi_i(r, E_i) r^2 \Omega(q, r, q_n) dr,$$

where dA/dV is the volumic activity. The geometric reduction factor $\Omega(q, r, q_n)$ defined by Berger (13) depends on various contingencies arising from the geometry of Figure 4:

$$\text{Case 1: } q < q_n \quad \Omega = \begin{cases} 1, & r \leq q_n - q \\ q_n^2 - (r - q)^2 / 4rq, & q_n - q < r \leq q + q_n \\ 0, & r > q + q_n \end{cases}$$

$$\text{Case 2: } q > q_n \quad \Omega = \begin{cases} 0, & r \leq q_n - q \\ q_n^2 - (r - q)^2 / 4rq, & q - q_n < r \leq q_n + q \\ 0, & r > q + q_n \end{cases}$$

For source distributions on cell membranes, the dose rate was directly integrated over the spherical surface using the relationship proposed by Langmuir (18):

$$\dot{D}(q) = \frac{q_c^2}{2} \frac{dA}{dS} k \sum_{i=1}^m n_i E_i \int_0^\pi \Phi_i(r(\theta), E_i) \sin \theta \, d\theta,$$

where dA/dS is the surfacic activity and q_c the radius of the cell. $r(\theta)$ verifies the equation: $r^2(\theta) = q_c^2 + q^2 - 2q_c q \cos \theta$.

REFERENCES

- Bassano DA, Mc Afee JG. Cellular radiation doses of labeled neutrophils and platelets. *J Nucl Med* 1979;20:255-259.
- Makrigrigors GM, Ito S, Baranowska-Kortylewicz J, et al. Inhomogeneous deposition of radiopharmaceuticals at the cellular level: experimental evidence and dosimetric implications. *J Nucl Med* 1990;31:1358-1363.
- Kassis AL, Adelstein SJ, Haydock C, Sastry KSR. Radiotoxicity of ^{75}Se and ^{35}S : theory and application to a cellular model. *Radiat Res* 1980;84:407-425.
- Makrigrigors GM, Adelstein SJ, Kassis AL. Limitation of conventional internal dosimetry at the cellular level. *J Nucl Med* 1989;30:1865-1864.
- Gardin I, Colas-Linhart N, Petiet A, Bok B. Dosimetry at the cellular level of Kupffer cells after technetium-99m-sulphur colloid injection. *J Nucl Med* 1992;33:380-384.
- Meignan M, Charpentier B, Wirquin E, Chavaudra J, Fries D, Galle P. Biological effects and irradiation dose induced in human lymphocytes in vitro by an intracellular radionuclide: ^{99m}Tc . *Radiat Res* 1983;94:263-279.
- Ten Berge RJM, Natarajan AT, Hardeman MR, Van Royen EA, Schellekens PTA. Labeling with ^{111}In has detrimental effects on human lymphocytes: concise communication. *J Nucl Med* 1983;18:1012-1019.
- Merz T, Tatum J, Hirsch J. ^{99m}Tc labeled lymphocytes: a radiotoxicity study. *J Nucl Med* 1986;27:105-110.
- Hofer KG, Hughes WL. Radiotoxicity of intracellular tritium, ^{125}I and ^{131}I . *Radiat Res* 1971;47:94-104.
- Rao DV, Narra VR, Howell RW, Lanka VK, Sastry KSR. Induction of sperm head abnormalities by incorporated radionuclides: dependence on subcellular distribution, type of radiation, dose rate, and presence of radioprotectors. *Radiat Res* 1991;125:89-97.
- Hofer KG, Harris CR, Smith JM. Radiotoxicity of intracellular ^{67}Ga , ^{125}I , and ^3H : nuclear versus cytoplasmic radiation in murine L1210 leukaemia. *Int J Radiat Biol* 1975;28:225-241.
- Germain D, Gentilhomme O, Bryon PA, Coiffier B. Cellules sanguines et organes hématopoïétiques. In: Simep SA, ed. *Physiologie humaine*. Paris: Villeurbanne; 1981:184-247.
- Berger MJ. Beta ray dosimetry calculation with the use of points kernels. In: Cloutier RJ, Edwards E, Snyder WS, eds. *Medical radionuclides: radiation dose and effects*. Conf-691212. Oak Ridge, TN: Oak Ridge National Laboratory; 1970:63-86.
- Prestwich WV, Chan L, Kwok CS, Wilson B. Dose point kernels for beta emitting radio-isotopes. *Proceedings of the 4th international radiopharmaceutical dosimetry symposium*. Conf-851113. Oak Ridge; 1985:545-561.
- Prestwich WV, Nunes J, Kwok CS. Beta dose point kernels for radionuclides: potential use in radioimmunotherapy. *J Nucl Med* 1989;30:1036-1046.
- Berger MJ. Improved point kernels for electron and beta ray dosimetry. *NBSIR*. Washington, DC: US Dept. of Commerce, National Bureau of Standards; 1973:73-107.
- Howell RW. Radiations spectra for Auger-electron emitting radionuclides: report no. 2 of AAPM nuclear medicine task group no. 6. *Med Phys* 1992;19:1371-1383.
- Langmuir VK, Sutherland RM. Dosimetry models for radioimmunotherapy. *Med Phys* 1988;15:867-873.
- De Labriolle-Vaylet C. Aspects radiobiologiques du marquage des leucocytes par le HMPAO- ^{99m}Tc chez l'homme. PhD dissertation, 1991.
- Gardin I, Faraggi M, Bok B. Cellular study of the energy delivered by electrons derived from ^{99m}Tc , ^{125}I , ^{111}In , ^{67}Ga and ^{201}Tl in a point source model: comparison with electromagnetic radiation. *J Med Nucl Biophys* 1992;16:342-347.
- Simpkin DJ, Mackie TR. EGS4 Monte Carlo determination of the beta dose kernel in water. *Med Phys* 1990;17:179-186.
- Howell RW, Rao DV, Sastry KSR. Macroscopic dosimetry of radioimmunotherapy: nonuniform activity distributions in solid tumors. *Med Phys* 1989;16:66-74.
- Cole A. Absorption of 20-eV to 50,000-eV electron beams in air and plastic. *Radiat Res* 1969;38:7-33.

24. Weber DA, Eckerman KF, Dillman LT, Ryman JC. In *MIRD radionuclides data and decay schemes*. New York: Society of Nuclear Medicine; 1989.
25. International Commission on Radiation Protection. Radionuclide transformations: energy and intensity of emissions. In: *ICRP publication 38*. New York: Pergamon Press, 1983.
26. Rao DV, Narra VR, Howell RW, Lanka VK, Sastry KSR. Biological consequence of nuclear versus cytoplasmic decays of ^{125}I : cysteamine as a radioprotector against Auger cascades in vivo. *Radiat Res* 1990;124:188–193.
27. Narra VR, Howell RW, Harapanhalli RS, Sastry KSR, Rao DV. Radiotoxicity of some iodine-123, iodine-125 and iodine-131-labeled compounds in mouse testes: implications for radiopharmaceutical design. *J Nucl Med* 1992;33:2196–2201.